Molecular Dynamics Study of the Early Intermediates in the Bacteriorhodopsin Photocycle

William Humphrey, Dong Xu, Mordechai Sheves,[1] and Klaus Schulten*,[2]

Beckman Institute and Departments of Physics and Biophysics, University of Illinois at Urbana-Champaign, 405 North Matthews, Urbana, Illinois 61801

Received: May 24, 1995; In Final Form: July 19, 1995[⊗]

The early stages of the bacteriorhodopsin photocycle, including the J_{625}, K_{590}, and L_{550} intermediates and the role of water molecules within the protein interior, are studied by means of molecular dynamics simulations. Our calculations examine two models for the excited state potential surface governing the observed *all-trans* → 13-*cis* photoisomerization: one surface hindering a $C_{14}-C_{15}$ single-bond corotation and the other surface allowing such corotation. The investigations use as a starting structure a model of bacteriorhodopsin based on electron-microscopy studies and subsequent molecular dynamics refinement. The following questions are addressed: How does the binding site guide retinal's photoisomerization? How does the photoisomerization depend on features of the excited state potential surface? Can one recognize a J_{625} intermediate? How does water participate in the early part of the pump cycle? How is the initial photoreaction affected by a lowering of temperature? To model the quantum yield, i.e., the dependence of the dynamics on initial conditions, 50 separate isomerization trials are completed for each potential surface, at both 300 and 77 K, the trials being distinguished by different initial, random velocity distributions. From these trials emerge, besides *all-trans*-retinal, three different photoproducts as candidates for the K_{590} intermediate: (1) 13-*cis*-retinal, with the Schiff base proton oriented toward Asp-96; (2) 13-*cis*-retinal, highly twisted about the C_6-C_7 bond, with the Schiff base proton oriented perpendicular to the membrane normal; (3) 13,14-*dicis*-retinal, with the Schiff base proton oriented toward the extracellular side. Two candidates for the K_{590} intermediate, case 2 and case 3 above, were subjected to simulated annealing to determine corresponding L_{550} structures. We suggest that photoproduct 2 above most likely represents the true K_{590} intermediate. Water molecules near the Schiff base binding site are found to play a crucial role in stabilizing the K_{590} state and in establishing a pathway for proton transfer to Asp-85.

Introduction

The protein bacteriorhodopsin (bR)[3] spans the cell membrane of *Halobacterium halobium* and functions as a light-driven proton pump. bR contains seven α-helices which enclose the prosthetic group, *all-trans*-retinal, bound via a protonated Schiff base linkage to Lys-216. The structure of bR and its retinal chromophore is shown in Figure 1. Retinal absorbs light and undergoes a photoisomerization process; the thermal reversal of this reaction is coupled to transfer of a proton from the cytoplasmic side (top of Figure 1) to the extracellular side (bottom of Figure 1) of the protein. Recent reviews discuss the structure and function of bR.[4-9]

Although bR is a small membrane protein, it conjoins for its bioenergetic function a multitude of properties: it is a pigment; it transports protons; it is extraordinarily stable under intense light yet undergoes continuously a cyclic reaction process; its consecutive reaction steps extend from extremely fast (500 fs for the initial photoisomerization) to slow (a complete cycle lasts a few milliseconds).[10] bR's most intriguing attribute may be that it has resisted a two-decades-long intense research effort and has not revealed the riddle of its pump mechanism. This is surprising, since (i) this mechanism apparently is closely tied to retinal, which can be observed well through resonance Raman and Fourier transform infrared (FTIR) spectroscopy, since (ii) the protonation states of key amino acid side groups can be monitored well, and since (iii) the protein exhibits only small conformational transformations during its pump cycle. The solution of bR's structure by Henderson *et al.*[11] has been a major advance, since it established a logical arrangement of the essential amino acids involved in the pump cycle, but this structure has not yet been able to reveal bR's pump mechanism.

We believe that the mechanism of bR's pump cycle has been elusive due to the fact that observations have not revealed a key player in the pump cycle, water. bR is known to contain water molecules;[12] their hydrogen-bond network with each other, with retinal, and with amino acid side groups should play a key role in proton transport. One needs to know where these water molecules are located in bR and how they participate in the pump cycle. The water molecules might rearrange during the pump cycle, open and close proton pathways, and, thereby, support the vectorial character of the pump. Another obstacle toward our understanding of bR's pump mechanisms is a lack of knowledge of the exact geometry of retinal in the early intermediates of the pump cycle. This geometry is mechanistically crucial, since retinal transfers a proton from its Schiff base nitrogen to Asp-85 and, eventually, to bR's extracellular side (bottom of Figure 1) and receives a proton from Asp-96 and, eventually, from bR's cytoplasmic side (top of Figure 1). However, according to the structure reported by Henderson *et al.*, a pure *all-trans* → 13-*cis* photoisomerization, as suggested by a straightforward interpretation of observations, would render the Schiff base nitrogen with its proton pointing in the wrong, i.e., upward, direction during the initial stage of the pump cycle.

Retinal's Schiff base binding site contains a complex counterion including Arg-82, Tyr-57, Tyr-185, Trp-86, and negatively charged Asp-85 and Asp-212.[11,13-16] It has been suggested that water molecules, within this binding site, participate in a hydrogen-bond network connecting the stated residues and the Schiff base proton (SBP).[12,13,17-20] FTIR data suggest that a water molecule, weakly hydrogen-bonded to the Schiff base in

[⊗] Abstract published in *Advance ACS Abstracts*, September 1, 1995.

0022-3654/95/2099-14549$09.00/0

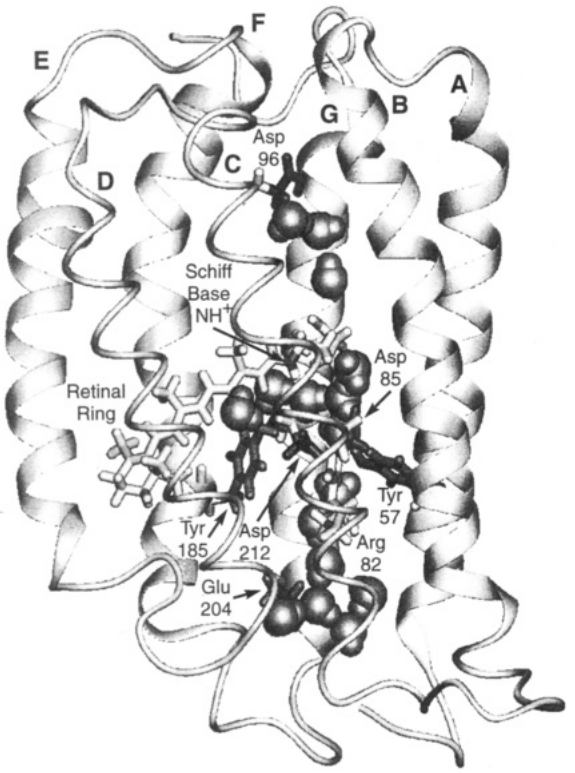

Figure 1. Ribbon diagram of bacteriorhodopsin, showing residues which are implicated in the proton pump mechanism. Water molecules placed within the protein interior are represented as solid spheres. Helices C and D are shown as thin ribbons to reveal the retinal binding site.

the wild type, forms a hydrogen-bond with both the Schiff base and Asp-85 in L_{550}.[20,21] The structure and function of water molecules within the interior of bR have been explored in several recent molecular dynamics (MD) studies.[22,23] Water molecules were seen to play an important role in these studies in regulating the distance between the SBP and Asp-85/Asp-212. In addition, water molecules were observed to form hydrogen-bond chains suitable for proton transport, e.g., between Arg-82 and Glu-204. The exact number, location, and orientation of water molecules suggested in these studies, however, is by no means definitive.

The proton pump cycle of bR proceeds through a series of intermediates identified by distinct absorption maxima. The early intermediates comply with the scheme[10]

$$bR_{568} \rightarrow J_{625} \rightarrow K_{590} \leftrightarrow L_{550} \quad (1)$$

where the subscript refers to the observed absorption maximum for each intermediate. The subsequent, late intermediates proceed through the sequence[10,24-27]

$$L_{550} \leftrightarrow M_{(I)412} \rightarrow M_{(II)412} \leftrightarrow N_{520} \leftrightarrow O_{640} \rightarrow bR_{568} \quad (2)$$

on a millisecond time scale. The exact nature of the photocycle kinetics, however, is still a topic of debate.

Our focus in this article is on the intermediates in reaction 1. After light absorption and photoisomerization of retinal, bR_{568} passes within 500 fs through the J_{625} intermediate to form, after 3−4 ps, the K_{590} intermediate.[28-30] K_{590} converts to L_{550} after 1−2 μs.[10,31] Due to its short lifetime, J_{625} is poorly characterized. It has been stated that retinal is in a 13-*cis* state in J_{625}, K_{590}, and L_{550};[32,33] i.e., these three intermediates involve a 180° torsion around retinal's $C_{13}-C_{14}$ bond. Time-resolved resonance Raman spectroscopy indicates that conformational changes accompany the $J_{625} \rightarrow K_{590}$ transition.[34,35] The K_{590} and the L_{550} intermediates can be stabilized at low temperature; the J_{625} intermediate cannot be stabilized under any known conditions.

The key determinant for bR's photoreaction $bR_{568} \rightarrow K_{590}$ is the excited state potential energy surface of retinal and its crossings with the ground state surface. Despite the ubiquitous occurrence of photoisomerization processes in polyene-type compounds, strikingly little is known about the potential surfaces involved, neither the number of states contributing surfaces nor the shape of the surfaces. This situation is compounded by the fact that polyene electron systems pose a formidable challenge to quantum chemistry due to the highly correlated nature of the involved electronic states, which requires extended multielectron basis sets for suitable description.[36] *Ab initio* quantum chemical methods, at present, cannot determine the relevant excited state potential energy surfaces for electron systems of the size found in retinal. A combined QM/MM technique such as the QCFF/PI method, which has been applied to the study of the photoisomerization event in rhodopsins,[37,38] does allow determination of an excited state potential surface which takes into account the surrounding chromophore−protein interactions. While computationally feasible for a system the size of bR, it is hard to judge the accuracy of the resulting surfaces and non-Born−Oppenheimer terms; in this respect we need to keep in mind that a definitive calculation would require a multidimensional potential surface at an accuracy of about 1 kcal/mol at any point. A rational, straightforward approach, at present, is to use simple model potential surfaces in MD simulations in order to learn how such surfaces, together with sterical effects of retinal's binding site and effects of inertia, determine retinal's photoproducts.

We investigate below two excited state potential surfaces, both of which induce an isomerization around retinal's $C_{13}-C_{14}$ double bond. One surface disfavors a concurrent isomerization around retinal's $C_{14}-C_{15}$ single bond through a large energy barrier; the other surface permits such isomerization. The chosen excited state potential surfaces reflect two models proposed for the photoisomerization process of retinal in bR, an *all-trans* → 13-*cis*, 14-*trans* reaction[39,40] or an *all-trans* → 13,14-*dicis* reaction.[25,41-44]

The observation of a quantum yield of the bR photoisomerization process of 0.64 ± 0.04,[45-47] i.e., of significantly less than unity, implies that the photoreaction of bacteriorhodopsin has a stochastic attribute. Accordingly, one needs to investigate how much the simulated photoisomerization depends on initial conditions as represented, e.g., through different random initial atomic velocities.

In this paper we address then the following questions connected with the intermediates in reaction 1: How do features of the excited state potential surface determine the photoisomerization products? How does the binding site guide retinal's photoisomerization? How does the initial photoprocess depend on initial conditions? How does water participate in the early intermediates? Can one recognize a J_{625} intermediate? What distinguishes the K_{590} and L_{550} intermediates? How do the initial steps depend on temperature? In the Methods section we introduce the excited state potential surfaces employed in our simulations as well as the molecular dynamics and annealing methods used. We also introduce a notation characterizing the different simulations carried out. In the Results section the simulations of photoproducts up to the L_{550} stage are presented for the two potentials used. In the Discussion section the results are analyzed in terms of the known bR structure, the involvement of waters, and proton transfer paths. The Conclusions section summarizes the key results of this paper and suggests future studies.

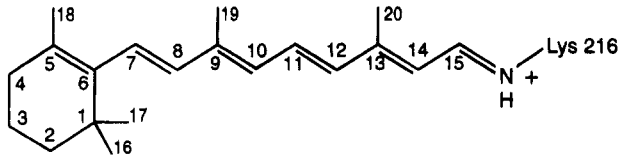

Figure 2. Retinal atom-numbering scheme.

TABLE 1: Retinal Partial Charges

atom	charge	atom	charge	atom	charge
N	−0.47	H_{SB}	0.38	C_{11}	−0.09
H	0.31	C_1	−0.07	C_{12}	−0.18
C	0.51	C_2	−0.26	C_{13}	0.13
O	−0.51	C_3	−0.28	C_{14}	−0.22
C_α	0.07	C_4	−0.33	C_{15}	0.20
H_α	0.09	C_5	0.02	C_{16}	−0.40
C_β	−0.18	C_6	0.12	C_{17}	−0.40
C_τ	−0.18	C_7	−0.17	C_{18}	−0.48
C_δ	−0.18	C_8	−0.14	C_{19}	−0.49
C_ϵ	−0.04	C_9	0.11	C_{20}	−0.49
N_{SB}	−0.63	C_{10}	−0.19		

Methods

Molecular dynamics simulations reported here are based on the refined and equilibrated structure of bR reported by Humphrey *et al.*[23] derived from the structure reported by Henderson *et al.*[11] Following Humphrey *et al.*[23] the present description involves explicit hydrogens, includes sixteen water molecules placed and equilibrated within the protein interior, and assigns standard protonation states to all side groups, except to Asp-96 and Asp-115, which are assumed to be protonated.[22,48] The water molecules are modeled using TIP3P parameters.[49] The program X-PLOR[50] with the CHARMm force field[51] was used for all simulations. bR was modeled in vacuum at temperatures of 77 and 300 K. A cutoff distance of 8 Å and a dielectric constant of $\epsilon = 1$ were used for the evaluation of Coulomb forces. All simulations use the standard X-PLOR protein topology file topallh6x.pro and parameter file parmallh3x.pro to model bR. The retinal topology and parameters for the equilibrium (bR_{568}) configuration are the same as used by Humphrey *et al.*,[23] with the exception of the $C_{15}-C_N$ dihedral energy barrier, which was increased to 30 kcal/mol to inhibit rotation about this bond during the isomerization process. Table 1 lists the partial charges assigned to retinal atoms; these charges were determined with Gaussian92,[52] using a Mulliken populational analysis at the MP2/6-31G level. Figure 2 describes the retinal atom-numbering scheme.

The potential surfaces assumed in the modeling of the initial photoisomerization of retinal differ in their dependence on the $C_{14}-C_{15}$ dihedral angle. Earlier studies[22,53] had employed for this purpose a schematic potential which combined the excited state and the ground state into a single surface. In the present study, the three phases of photoisomerization, shown schematically in Figure 3, namely, excited state dynamics (phase I), surface crossing (phase II), and ground state dynamics (phase III), are described through three separate surfaces. The potential for phase I, governing steps a and b in Figure 3, is modeled through a surface with a maximum at the *trans* and *cis* positions of the $C_{13}-C_{14}$ dihedral angles and a minimum at the 90° twist of this bond. The nonadiabatic crossing from the excited state to the ground state potential surface in phase II, i.e., step c in Figure 3, is modeled through a $C_{13}-C_{14}$ bond dihedral angle potential with a single minimum at 13-*cis*. For phase III, i.e., step d in Figure 3, the conventional dihedral potential is reinstated.

The surfaces are modeled through simple analytical expressions governing the dependence of the energy on the dihedral angles ϕ_1 and ϕ_2 of retinal's $C_{13}-C_{14}$ and $C_{14}-C_{15}$ bonds,

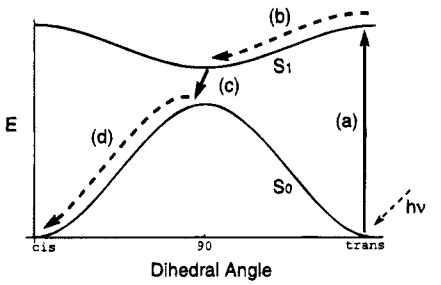

Figure 3. Schematic representation of the photoexcitation of retinal and subsequent isomerization. bR absorbs a photon *hv* and is excited from its electronic ground state S_0 to its excited state S_1. (a) S_1 has a potential surface with a minimum near the S_0 maximum. After promotion to the S_1 surface retinal moves to the minimum of this surface within 200−300 fs. (b) Retinal then crosses back to the ground state, i.e., S_0, surface. (c) On the latter surface retinal completes the *trans*−*cis* isomerization (d).

TABLE 2: Equilibrium (Phase III) Parameters Used for the Torsional Potentials of Retinal

ϕ_i	k_i (kcal/mol)	n_i	δ_i (deg)
$C_5-C_6-C_7-C_8$	5.0	2	176.6
$C_6-C_7-C_8-C_9$	30.0	2	176.6
$C_7-C_8-C_9-C_{10}$	5.0	2	176.6
$C_8-C_9-C_{10}-C_{11}$	30.0	2	176.6
$C_9-C_{10}-C_{11}-C_{12}$	5.0	2	176.6
$C_{10}-C_{11}-C_{12}-C_{13}$	30.0	2	176.6
$C_{11}-C_{12}-C_{13}-C_{14}$	5.0	2	176.6
$C_{12}-C_{13}-C_{14}-C_{15}$	25.2	2	176.6
$C_{13}-C_{14}-C_{15}-N_{SB}$	10.0	2	176.6
$C_{14}-C_{15}-N_{SB}-C_\epsilon$	30.0	2	176.6

TABLE 3: Parameters Used in Eq 3

	phase I			phase II		
i	k_i (kcal/mol)	n_i	δ_i (deg)	k_i (kcal/mol)	n_i	δ_i (deg)
			13-*cis* Isomerization			
1	−25.2	2	180.0	50.4	1	180.0
2	10.0	2	176.6	10.0	2	176.6
			13,14-*dicis* Isomerization			
1	−25.2	2	180.0	25.2	1	180.0
2	1.0	2	176.6	25.2	1	180.0

respectively. For this purpose additive contributions $E_1^{dihe} + E_2^{dihe}$ were assumed, with the two terms given by

$$E_i^{dihe} = \frac{1}{2}k_i[1 + \cos(n_i\phi_i + \delta_i)] \quad (3)$$

Table 2 provides the potential energy parameters for the ground state (phase III), and Table 3 provides the parameters for phase I and II potentials. Figures 4 and 5 illustrate the potential energy surfaces. The potentials are chosen such that the transition from the initial ground state (phase III) potential to the phase I potential, i.e., step a in Figure 3, imparts on retinal (in an *all-trans* geometry) 50.4 kcal/mol, which corresponds to the energy of a 568 nm photon. It is important to note that this energy, according to our model, is stored at the beginning of phase I solely in the degree of freedom of torsional rotation about the $C_{13}-C_{14}$ bond.

To investigate a possible dependence of the photoisomerization on the initial state, 50 independent trials, characterized through independently chosen random velocities of all protein atoms, were carried out. Each trial started from the same bR_{568} structure but with different initial velocities chosen from a Maxwell distribution at 77 or 300 K. Simulations at 300 K involved an initial 100 fs of equilibration dynamics with a phase III potential, as shown in Figure 4a and 5a. Simulations at 77 K extended this equilibration to 5 ps, accounting for the need of a longer equilibration time, since the structure of bR_{568} was

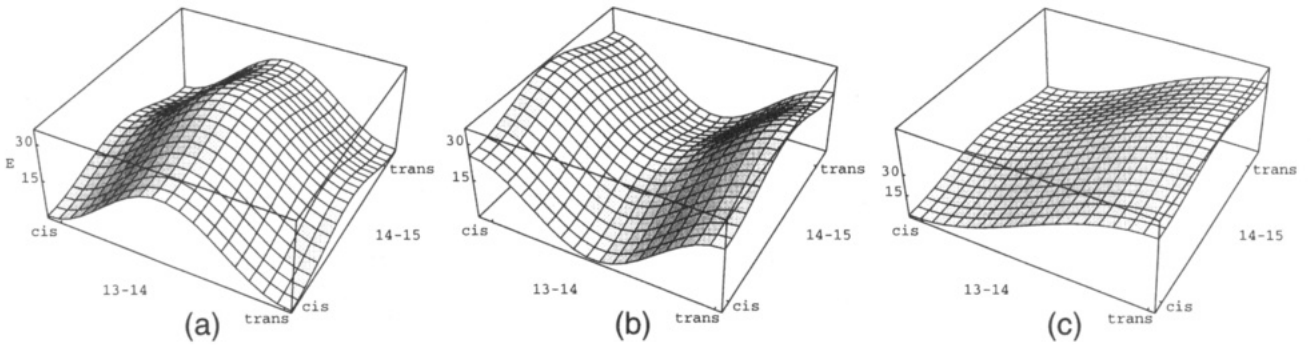

Figure 4. 13-*cis* potential energy surface for $C_{13}-C_{14}$ and $C_{14}-C_{15}$ dihedral angles: (a) equilibrium surface (phase III); (b) inverted-potential surface (phase I); (c) single-minimum surface (phase II).

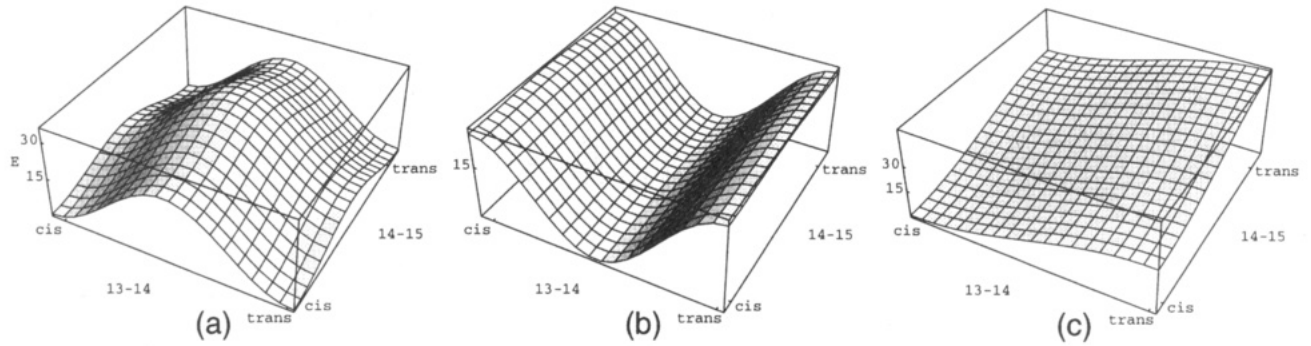

Figure 5. 13,14-*dicis* potential energy surface for $C_{13}-C_{14}$ and $C_{14}-C_{15}$ dihedral angles: (a) equilibrium surface (phase III); (b) inverted-potential surface (phase I); (c) single-minimum surface (phase II).

actually determined by earlier MD refinement at $T = 300$ K. Following the initial equilibration, for each trial the excited state (phase I) potential, as shown in Figures 4b and 5b, was applied for 250 fs. After this period the potential governing phase II of the photoprocess, as shown in Figures 4c and 5c, was applied for 250 fs. Finally, the ground state (phase III) potential function was restored and 4.5 ps of further dynamics completed. Restart files were used between each switch of potential functions to preserve the dynamical state.

Since the $K_{590} \rightarrow L_{550}$ transition requires a microsecond time period, which cannot be covered by molecular dynamics simulations, we employed simulated annealing,[54] using representative K_{590} structures (see below) as starting points. Simulated annealing is often applied at very high temperatures, typically 1000−4000 K.[55] Such high temperatures were found to adversely affect the structure of bR, and therefore, the maximum annealing temperature was limited to 500 K. The SHAKE algorithm[56] for bond-length constraints was used for simulations at $T > 300$ K, in order to maintain stable numerical integration with a 1 fs time step. Since dihedral angles of the single bonds of retinal's backbone become too flexible at high temperatures, during the annealing process torsional barriers of 5−10 kcal/mol for the C_6-C_7, C_8-C_9, $C_{10}-C_{11}$, and $C_{12}-C_{13}$ bonds of retinal were assumed to stabilize its geometry.

The temperature protocol used to determine the L_{550} intermediate is presented in Figure 6. First, torsional potentials for retinal were changed as described, and a 100-step conjugate gradient energy minimization calculation was carried out. Then, starting at $T_0 = 500$ K, the system was simulated for 100 fs using temperature coupling to rescale velocities to the appropriate temperature; for this purpose a frictional force

$$\vec{F}_j = -m_j \vec{v}_j \gamma (T_0/T - 1) \qquad (4)$$

with $\gamma = 100$ ps^{-1} was applied to each atom j with mass m_j and velocity $\vec{v}_j$. This was followed by a 50-step conjugate gradient energy minimization. The annealing calculations were repeated at 10 K intervals from 500 to 300 K. The frequent

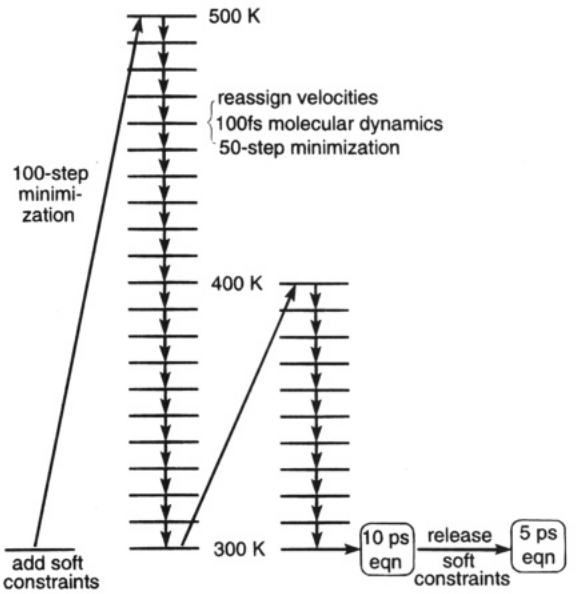

Figure 6. Temperature protocol of the simulated annealing process. The label "eqn" refers to a conventional molecular dynamics simulation at 300 K. Soft constraints refer to a change of torsional potentials of retinal which are invoked to keep retinal planar during the annealing process and are released thereafter.

velocity reassignment facilitated a wider search of conformation space, and the energy minimization helped avoid instabilities. After a temperature of 300 K was reached, an analogous annealing cycle was started at 400 K, reducing temperatures again to 300 K. The annealing calculations were then followed by a 15 ps equilibration phase at 300 K.

Simulations $Al_{300}...A50_{300}$ and $A1_{77}...A50_{77}$ modeled the 13-*cis* photoisomerization and subsequent equilibration at 300 and 77 K, respectively, while simulations $B1_{300}...B50_{300}$ and $B1_{77}...B50_{77}$ modeled the 13,14-*dicis* photoisomerization and equilibration at 300 and 77 K. The numbers 1−50 refer to the specific trial run, and the subscripts 300 and 77 refer to the

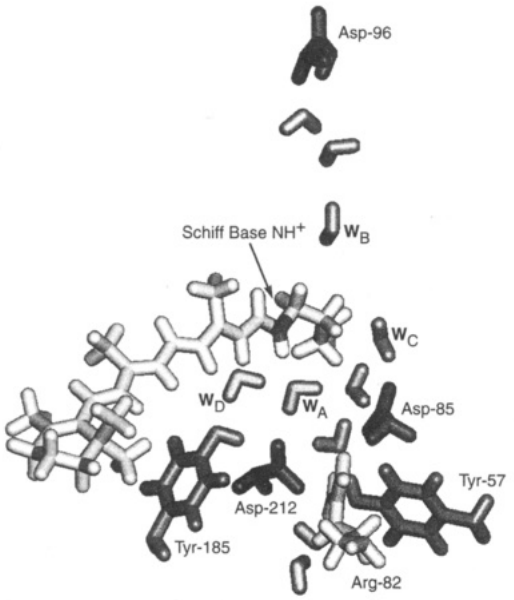

Figure 7. Structural features of the binding site for the starting structure used in all isomerization trials.

modeled temperature. One representative structure, from simulations $A1_{300}...A50_{300}$ and $B1_{300}...B50_{300}$, referred to below as K_1 and K_2, was selected as a starting point for the annealing process outlined above to describe the 2 μs $K_{590} \rightarrow L_{550}$ transition. Simulation C, which resulted in structure L_1 starting from K_1, describes the 13-*cis* model; simulation D, resulting in structure L_2 starting from K_2 describes the 13,14-*dicis* model.

Results

Figure 7 illustrates the key features of the binding site of bR for the initial structure used in all isomerization simulations. Within this structure, four water molecules (W_A, W_B, W_C, W_D) make direct hydrogen-bonding contact with the SBP, either before or after the isomerization process. W_A is directly hydrogen-bonded to the SBP in the starting structure. W_B is located above the SBP toward the cytoplasmic side of the membrane and is part of a chain of three water molecules (W_{B1}, W_{B2}, W_{B3}) connected to Asp-96. W_C is in the region between the SBP and Asp-85 and makes a hydrogen-bond with Thr-89 (not shown), as well as with Asp-85 and another water molecule. W_D is near the SBP, outside of hydrogen-bond contact, but still below the Schiff base toward the extracellular side of the membrane. W_D is involved in a hydrogen-bond with W_A and also with Tyr-185.

It was observed in our simulations of excited state and potential crossing dynamics that the orientation of the $N-H^+$ Schiff base bond, after isomerization and equilibration, assumed basically one of three possible configurations: $N-H^+$ pointing "up", i.e., toward the cyotplasmic side of bR; $N-H^+$ pointing "down", i.e., toward the extracellular side of bR; and $N-H^+$ pointing roughly perpendicular to the membrane normal. To measure this orientation, we define θ_{SB} as the angle between a line formed by $N-H^+$ and a line connecting the Schiff base nitrogen and the Asp-96 carboxyl: for small θ_{SB}, $N-H^+$ points toward Asp-96, while, for $\theta_{SB} \approx 180°$, the orientation of $N-H^+$ is toward the extracellular side of the protein. For each set of 50 trials, the photoisomerization products were grouped into one of four cases on the basis of the value of θ_{SB} and the configuration of the $C_{13}-C_{14}$ and $C_{14}-C_{15}$ dihedral angles. The definitions of these cases are given in Table 4. This table also lists the percentage of occurrence for simulations $A1_{300}...A50_{300}$, $B1_{300}...B50_{300}$, $A1_{77}...A50_{77}$, and $B1_{77}...B50_{77}$ (see Methods for definitions of these simulations). Figure 8 provides illustrations

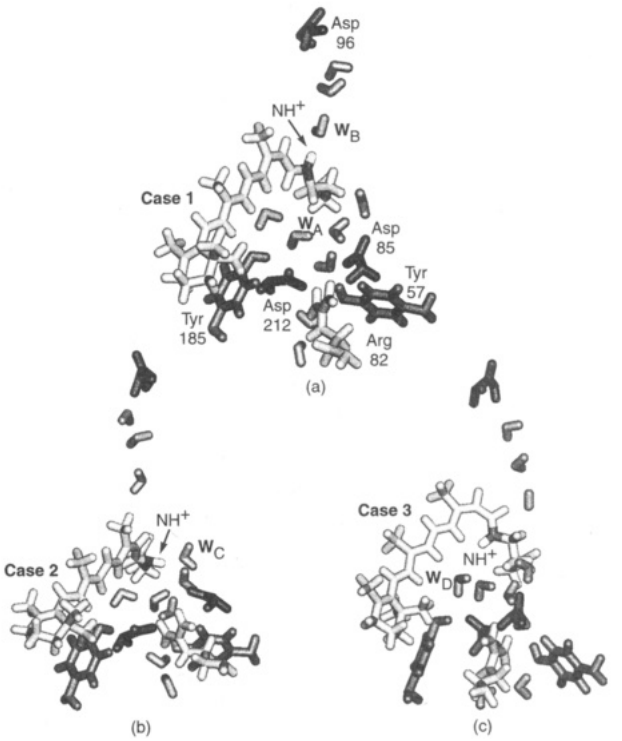

Figure 8. Photoisomerization products observed in simulations $A1_{300}...A50_{300}$ and $B1_{300}...B50_{300}$: (a) case 1; (b) case 2; (c) case 3.

TABLE 4: Definitions of Cases Used To Categorize Isomerization Trials, and Percentage of Cases Present in Each Set of Simulations

		300 K		77 K	
case	definition	13-*cis*	13,14-*dicis*	13-*cis*	13,14-*dicis*
1	13-*cis*, $\theta_{SB} \leq 60°$	58	12	72	0
2	13-*cis*, $\theta_{SB} > 60°$	36	2	0	0
3	13,14-*dicis*, $\theta_{SB} > 90°$	6	28	28	76
4	*all-trans*, $\theta_{SB} > 90°$	0	50	0	22

of the key features of representative case 1 (Figure 8a), case 2 (Figure 8b), and case 3 (Figure 8c) structures.

13-*cis* Isomerization Model. *300 K.* According to the textbook model of an *all-trans* $\rightarrow$ 13-*cis* photoisomerization, retinal, after initial light excitation, rotates about its $C_{13}-C_{14}$ bond by 180° and leaves the $N-H^+$ bond oriented in the direction of Asp-96. However, Asp-96 acts as the proton donor rather than acceptor in the photocycle such that this orientation does not appear desirable from a mechanistic point of view. In 58% of simulations $A1_{300}...A50_{300}$, this orientation of $N-H^+$ is observed, and retinal photoisomerizes into a basically planar 13-*cis* conformation. In 36% of simulations $A1_{300}...A50_{300}$, however, the Schiff base photoisomerizes, such that the $N-H^+$ bond points roughly perpendicular to the membrane normal, midway between being oriented toward Asp-96 and being oriented in the original *all-trans* direction (toward the Asp-85/Asp-212/water counterion complex). Retinal accommodates this conformation through a series of twists about its single bonds, particularly, through a large twist about its C_6-C_7 bond. The resulting $N-H^+$ orientation is stabilized by a strong hydrogen-bond formed between $N-H^+$ and water W_C, such that the Schiff base participates in a direct hydrogen-bond chain to Asp-85, the acceptor for retinal's proton during the $L_{550} \rightarrow M_{412}$ transition.[57] The remaining 6% of simulations $A1_{300}...A50_{300}$ result in $N-H^+$ pointing toward the extracellular side, leaving retinal in a 13,14-*dicis* conformation, despite the large (10 kcal/mol) barrier for rotation about the $C_{14}-C_{15}$ bond.

Figure 9 shows the time evolution of various angles and distances which measure the configuration of retinal and

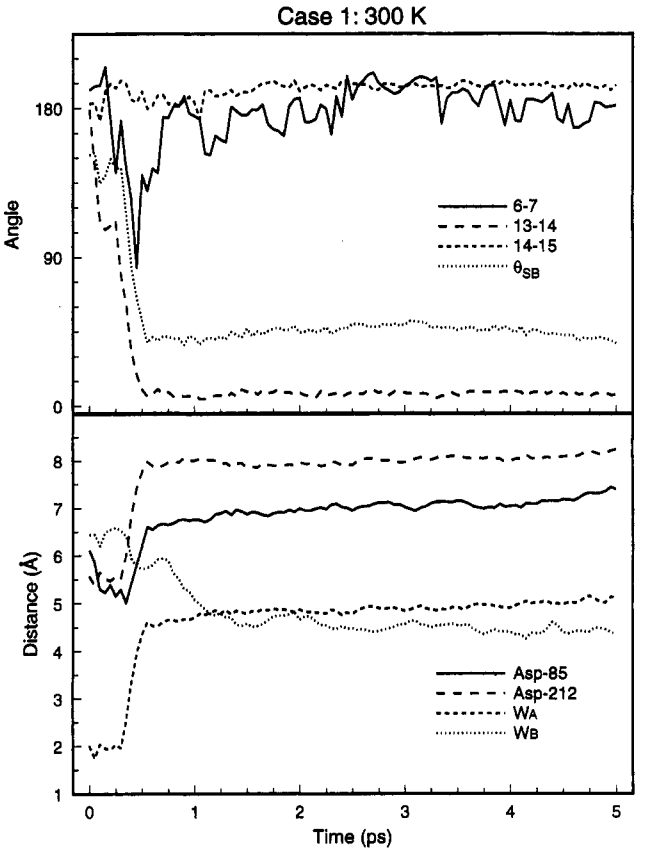

Figure 9. Averaged time evolution for case 1 trials in simulations $A1_{300}...A50_{300}$. The upper graph shows the values for retinal dihedral angles and θ_{SB} at 50 fs intervals, averaged over all trials classified as case 1. The lower graph gives the values for the distance of the aspartic acid carboxyl groups to the SBP and the distance of water molecules W_A and W_B to the SBP.

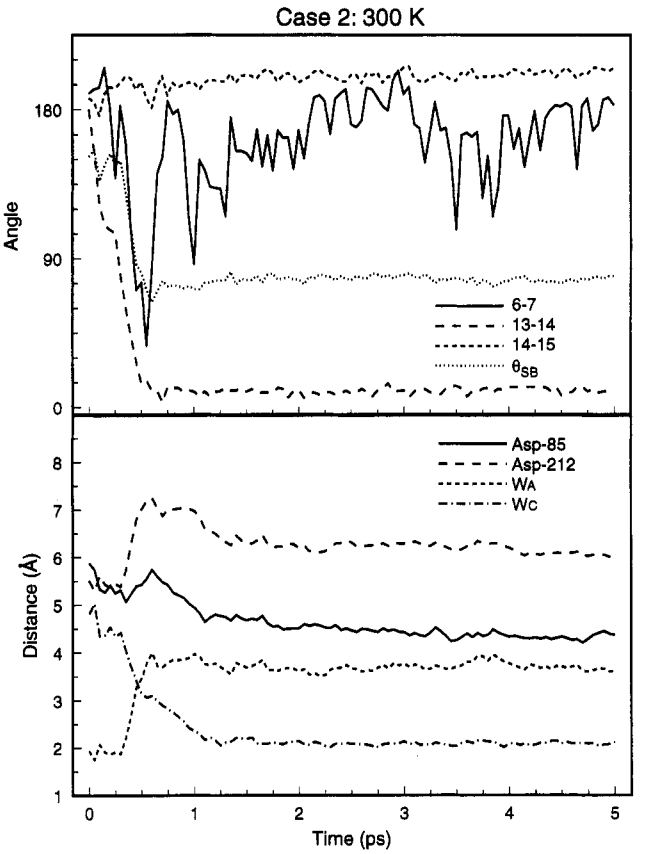

Figure 10. Averaged time evolution for case 2 trials in simulations $A1_{300}...A50_{300}$. The upper graph shows the values for retinal dihedral angles and θ_{SB} at 50 fs intervals, averaged over all trials classified as case 2. The lower graph gives the values for the distance of the aspartic acid carboxyl groups to the SBP and the distance of water molecules W_A and W_C to the SBP.

surrounding residues duruing the photoisomerization. The quantities shown are averages for all trials in simulations $A1_{300}...A50_{300}$ which resulted in case 1 structures, at 50 fs intervals. The upper graph in Figure 9 indicates the time evolution of the rotations about the C_6-C_7, $C_{13}-C_{14}$, and $C_{14}-C_{15}$ bonds and the value of θ_{SB} defined above. The lower graph in Figure 9 shows the average distance between the SBP and the Asp-85 and Asp-212 carboxyl groups. The lower graph also provides the distance from the SBP to waters W_A and W_B. The figure shows that the isomerization of case 1 trials completes within the first 500 fs, with θ_{SB} near 45°. Retinal experiences some twisting about the C_6-C_7 bond during the initial picosecond of simulation but returns to a mainly *trans* geometry for this bond during the final 4.5 ps. The distance from the SBP to both Asp-85 and Asp-212 increases during the case 1 simulation. Water W_A breaks its hydrogen-bond with the Schiff base very early, and water W_B (in the region between the Schiff base and Asp-96) moves closer to the SBP. In some trials, this water molecule moves close enough to hydrogen-bond to the Schiff base. However, on average, this water does not get close enough to make hydrogen-bond contact by the end of 5 ps.

The averaged time evolution results for case 2 outcomes of simulations $A1_{300}...A50_{300}$ are shown in Figure 10. In this case, the Schiff base forms a strong hydrogen-bond with water W_C, as clearly shown by the SBP$-W_C$ distance. This hydrogen-bond stabilizes the $N-H^+$ bond in a direction with $\theta_{SB} \approx 90°$. In Figure 10, the isomerization to 13-*cis* is seen to complete within the initial 500 fs, i.e., during phases I and II. However, retinal maintains a 15−20° twist about both the $C_{13}-C_{14}$ and $C_{14}-C_{15}$ bonds after isomerization. These twists, along with the observed large rotations about the C_6-C_7 single bond, allow retinal to maintain the $N-H^+$ bond oriented at a $\theta_{SB} \approx 90°$ angle. With retinal in this conformation, the distance from the SBP to Asp-85 decreases slightly by the end of the photoisomerization, whereas the distance to Asp-212 increases slightly.

77 K. Simulations $A1_{77}...A50_{77}$ studied the 13-*cis* isomerization reaction in the same manner as simulations $A1_{300}...A50_{300}$ but at 77 K. Experiments have shown that the K_{590} state can be trapped at this temperature, with little change in the spectral absorption maximum.[58] Table 4 lists the results for simulations $A1_{77}...A50_{77}$. Of the 50 trials, 72% result in case 1 structures, and the rest result in 13,14-*dicis* structures (case 3). In contrast to the simulations at 300 K, no case 2 photoproducts arise. Figure 11 shows the averaged time evolution for the case 1 structures with the 13-*cis* parameters at 77 K, the presentation corresponding to that in Figures 9 and 10 for the 300 K case. Only the angular quantities are shown here, to exemplify the low-temperature behavior as compared to the room-temperature behavior (cf. Figure 9, top). The dynamics for case 1 photoproducts is the same at 77 and 300 K but with much smaller deviations from the mean for 77 K. The photoisomerization completes also within 500 fs. The resulting θ_{SB} is about 45°, indicating an $N-H^+$ bond pointing toward Asp-96. Small initial perturbations about the C_6-C_7 bond arise within the first picosecond; retinal assumes eventually a nearly planar conformation. A similar behavior is seen for trials leading to case 3 photoproducts.

13,14-*dicis* Isomerization Model. *300 K.* The 13,14-*dicis* photoisomerization is modeled here in simulations $B1_{300}...B50_{300}$ by applying phase I and phase II potentials as described in the Methods and illustrated in Figure 5. In 50% of the simulations

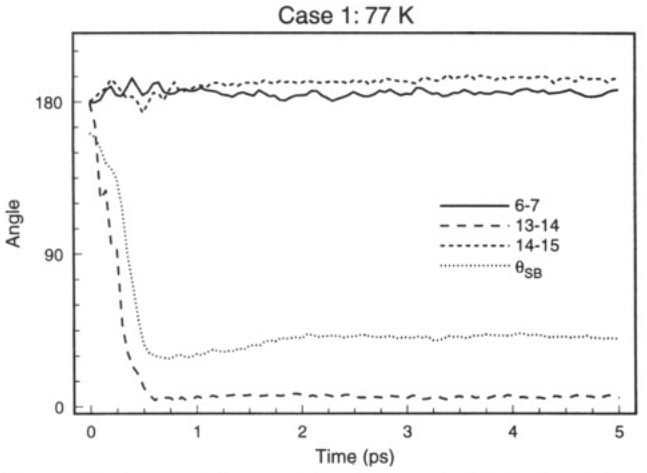

Figure 11. Averaged time evolution for case 1 trials in simulations $A1_{77}...A50_{77}$.

$B1_{300}...B50_{300}$, retinal did not complete the *all-trans* → 13,14-*dicis* photoisomerization, actually remaining instead in the *all-trans* (case 4) conformation. Of the remaining trials, 28% resulted in 13,14-*dicis* retinal with $N-H^+$ pointing toward the extracellular side, i.e., resulted in case 3, and 14% formed 13-*cis* (case 1 and case 2 structures). The remaining 8% of simulations $B1_{300}...B50_{300}$ resulted in a highly distorted 12,14-*dicis* retinal. There is no experimental evidence for the latter photoisomerization product.

Only 50% of the trials in simulations $B1_{300}...B50_{300}$ resulted in an isomerized retinal; of the runs which did succeed in converting native bR, over half formed a 13,14-*dicis* product (case 3). Figure 12 shows the averaged time evolution for these case 3 runs, the presentation corresponding to that in Figures 9 and 10. For this case, the isomerization completes within the first 500 fs. There arises some twist about the C_6-C_7 bond during the initial stage but this twist is reduced during the ensuing 4.5 ps of simulation. The orientation of $N-H^+$, as measured by θ_{SB}, remains toward the extracellular side of bR, i.e., $\theta_{SB} > 90°$. There is little to no twist about the $C_{13}-C_{14}$ and $C_{14}-C_{15}$ bonds after the first picosecond. In Figure 12, it is seen that both aspartic acid groups end up further away from the SBP after the 5 ps simulation, each by approximately 1 Å. Water W_D replaces water W_A as the Schiff base hydrogen-bond partner, and W_A moves further away from the Schiff base.

77 K. Molecular dynamics simulations $B1_{77}...B50_{77}$ were carried out at 77 K employing also the potential surfaces favorable for an *all-trans* → 13,14-*dicis* photoisomerization. The results are summarized in Table 4 as well. Of the 50 trials, 76% result in case 3 structures, with retinal in the expected 13,14-*dicis* isomeric state and the $N-H^+$ bond pointing to the extracellular side. Of the rest, 22% of the simulations did not complete the isomerization and returned to the *all-trans* state. In one case (2%) a 12,14-*dicis* product also was observed. None of the simulations produced a 13-*cis* product. This is due to the effect of the binding cavity, which favors an *all-trans* → 13,14-*dicis* photoisomerization. As in simulations $A1_{77}...A50_{77}$, the motion of retinal for the low-temperature simulations $B1_{77}...B50_{77}$ exhibits less deviation from the mean than in the case of the 300 K simulations. Key differences between simulations $B1_{77}...B50_{77}$ and $B1_{300}...B50_{300}$ are the much larger number of case 3 structures and the lack of 13-*cis* (cases 1 and 2) for 77 K.

Determination of L_{550}. As described in the Methods, simulated annealing was employed to bridge the 2 μs time scale, the respective simulations still being extremely time consuming. Therefore, only a single case 2 structure, termed K_1, was selected from $A1_{300}...A50_{300}$ and a single case 3 structure, termed K_2,

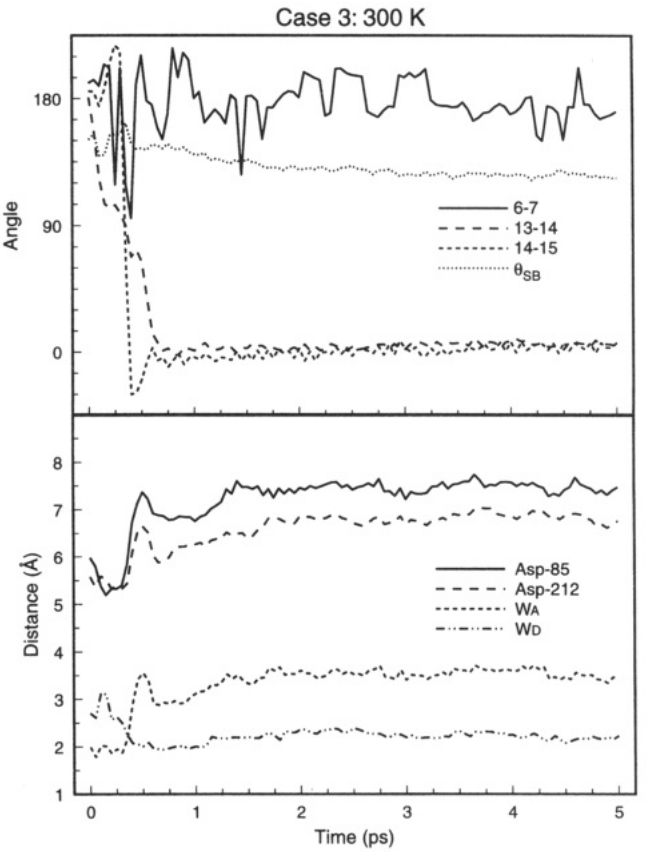

Figure 12. Averaged time evolution for case 3 trials in simulations $B1_{300}...B50_{300}$. The upper graph shows the values for retinal dihedral angles and θ_{SB} at 50 fs intervals, averaged over all trials classified as case 3. The lower graph gives the values for the distance of the aspartic acid carboxyl groups to the SBP and the distance of water molecules W_A and W_D to the SBP.

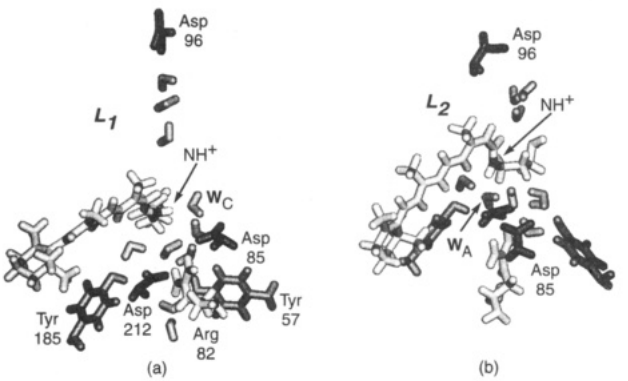

Figure 13. Retinal binding site region structural features for the simulated L_{550} intermediates: (a) L_1; (b) L_2.

was selected from $B1_{300}...B50_{300}$ as a starting point for two annealing calculations. The structures K_1 and K_2, taken from the final state after the 5 ps isomerization/equilibration dynamics, are considered candidates for the K_{590} state and, as starting points in simulations C and D, yield candidates for the L_{550} intermediate. The respective structures are denoted as L_1 and L_2. Figure 13 presents the configuration of the bR binding site region for L_1 and L_2.

During simulation C, the $N-H^+$ bond maintained its orientation perpendicular to the membrane normal, as indicated in Table 5. This table compares values for the orientation of the $N-H^+$ bond and for the distances from the SBP to the Asp-85/Asp-212 carboxyls in K_{590} and L_{550}. One can see that the nearby aspartic acids maintained nearly the same relative distance to the SBP during this simulation, while the Asp-212 distance decreased by only 0.4 Å. During simulation D, the $N-H^+$ bond

TABLE 5: Comparison of Retinal Configuration Data between bR_{568}, K_{590}, and L_{550} Intermediates from Simulations C (13-*cis*) and D (13,14-*dicis*)

	θ_{SB} (deg)	SBP−Asp-85 (Å)	SBP−Asp-212 (Å)
bR_{568}	158.2	5.71	5.42
K_{590} (case 2)	79.4	4.37	6.00
L_{550} (C)	80.7	4.17	5.57
K_{590} (case 3)	123.5	7.47	6.76
L_{550} (D)	117.6	6.44	4.36

remained pointing to the extracellular side of bR, indicating that retinal in both the K_{590} and the L_{550} intermediates maintained a 13,14-*dicis* configuration. However, during simulation D the separations between the SBP and the aspartic acid carboxyls of Asp-85 and Asp-212 decreased significantly; for example, the Asp-212 carboxyl moved 2.4 Å closer to the SBP.

Discussion

Simulations of the bR photocycle have been carried out previously, using both molecular dynamics methods[22,53] and combined QM/MM methods.[37,38] The present study differs in several aspects from the earlier MD investigations by Nonella *et al.* and Zhou *et al.*, namely, in that we start from an all-atom bR structure with a new placement of water molecules,[23] in that we employ a three-phase description of the photoisomerization process, and in that we carry out a series of fifty simulations for each model or temperature tested. The present study differs also from the earlier QM/MM studies, by using a classical approximation for the photoisomerization process and by using as a starting structure the refined bR_{568} structure described by Humphrey *et al.*.[23] Recently, molecular dynamics studies of the bR photocycle have been reported which also calculate the pK_a of the simulated intermediate structures.[59,60]

The quantum yield for formation of the K_{590} intermediate in the primary photoprocess of bR has been determined to be 0.64 ± 0.04.[45-47] The quantum yield is independent of temperature down to 108 K.[61] This yield implies that a majority, but not all, of the trajectories describing the photoprocess of bR result in an isomerized retinal. To account for this behavior we carried out molecular dynamics simulations on schematic potential surfaces describing the ground and excited states of retinal, rather than enforcing an isomerization, i.e., a quantum yield of unity, as done in previous studies.[22,53] Simulations were initially conducted with the phase II step (see Methods) eliminated and the phase I duration extended or reduced to 200, 300, 400, 500, 700 and 1000 fs. At most 5% of the respective trials completed the isomeriation to 13-*cis* or 13,14-*dicis*; most trials returned, instead, to the initial *all-trans* configuration after rotating to near 90° about the $C_{13}-C_{14}$ bond in phase I. We therefore applied a second potential to bias, in phase II (i.e., step c in Figure 3), retinal's torsion toward completion of the *all-trans* → 13-*cis* isomerization. Such a bias arises in the actual photochemistry if the crossing point of the S_1 and S_0 states is shifted toward the *cis* geometry or if the actual surface crossing process favors the direction *all-trans* → 13-*cis*. Deflection of *trans* → *cis* isomerization reactions back toward the *trans* configuration has been found also in previous simulation studies.[37,38] It is possible that the observed deflections in this study are the result of the particular potential energy surface used, which may not include all relevant torsional mode couplings.

The results of simulations with different initial conditions predict that the bR quantum yield may result from several similar photoisomerization reaction pathways, only a subset of which leads to a cycle which actually pumps protons. It is as yet not clear if the heterogeneity of photoisomerization products emerging in our simulations is an artifact, e.g., due to the schematic potential surfaces used, or if these products correspond to multiple cylces all occuring at the same time, as has been suggested.[62-64]

J_{625} Intermediate. Relatively little data have been acquired for the J_{625} intermediate, in part, due to its short lifetime of 5 ps.[30] Resonance Raman spectroscopy at 3 ps resolution has indicated that photoisomerization to the J_{625} state results in strong hydrogen-out-of-plane (HOOP) motion which decreases within 4 ps as the protein converts to K_{590}.[35] In all simulations which complete the photoisomerization, photoproducts appeared within the first 500 fs, i.e., within the time period over which phase I and II potentials were applied. The fast changes during this time affected hydrogen-bonds between the Schiff base and surrounding water molecules as well as twists of retinal's single and double bonds. Between 500 fs and 5 ps, i.e., the time of formation of the K_{590} intermediate, little structural change was seen.

The actual existence of a structurally distinct J_{625} state is still controversial. Recent work has hinted at the possibility that the J_{625} state intermediate arises due to a dipole moment induced in bR through the charge shift connected with retinal's photoexcitation.[65] This suggestion precludes the need for specific structural changes from J_{625} to K_{590} and can explain why J_{625} cannot be trapped at low temperatures. Our simulations support this suggestion, due to the small amount of structural change seen in the 500 fs to 5 ps dynamics.

K_{590} Intermediate. In contrast to J_{625}, much is known about bR's K_{590} intermediate, which is blue-shifted relative to the preceding J_{625} state but is red-shifted relative to bR_{568}. This state is formed within 4 ps following the isomerization reaction and has been determined to involve a 13-*cis* retinal. Our simulations were conducted for 5 ps, i.e., over a time period which matches the observed time of K_{590} formation. The structure at the end of the 5 ps simulation period is associated with the K_{590} state.

Another observed change from J_{625} to K_{590} is a decrease of the intensity of HOOP modes,[35] which corresponds to an increase in the planarity of retinal. All three photoproducts, i.e., cases 1−3, experience a reduction in the twist about the C_6-C_7 bond in the final 4 ps of simulation. Case 3 exhibits a definite reduction in the oscillation of this C_6-C_7 twist, while case 1 does not show much change after the initial isomerization. Case 2 displays the largest oscillations and overall twist of the C_6-C_7 bond; this is true for the other dihedral angles along the retinal backbone as well (not shown). In Figure 10, the amplitude of these oscillations and the amount of twist for the C_6-C_7 bond decrease during the time from 500 fs to 3 ps and then show a slight increase in the 3−5 ps period. This might indicate that the K_{590} state has not stabilized for case 2 structures. Regardless, structural changes capable of explaining the observed HOOP modes in K_{590} compared to J_{625} are present in cases 2 and 3 and to a lesser degree in case 1.

An important feature of the K_{590} intermediate simulations is associated with the prediction that different structures are obtained at 300 and 77 K. This is actually in keeping with experimental data, which indicate different absorption maxima for the two species (590 and 603−606 nm, respectively)[29,66] and different resonance Raman spectra.[35] Both resonance Raman and FTIR spectra indicate strong HOOP intensities in the spectra of K_{590} at 77 K, which are attributed to twists around single bonds[67] or to a C=N out-of-plane twist.[68] However, the simulations of K_{590} at 77 K indicate a planar conformation adopted by the retinal chromophore. This discrepancy might indicate that the simulations do not describe accurately the retinal conformation in K_{590} at 77 K or that the HOOP intensity originates for another reason such as steric interaction with

neighboring residues. Calculations of the resonance Raman spectra for rhodopsin[37] have demonstrated the need to take into account the surrounding protein conformation restraints on the chromophore, suggesting that the observed HOOP intensities result in part from chromophore−protein strain.

L_{550} Intermediate. While the very short time scales of the $bR_{568} \rightarrow J_{625} \rightarrow K_{590}$ transitions allow us to directly simulate these events, modeling of the significantly longer $K_{590} \rightarrow L_{550}$ transition (of about 2 μs) relied on the simulated annealing method. Use of this method implies a loss of time scale, and we cannot claim that simulations C and D above cover a complete 2 μs transition period. The simulations do, however, provide structures significantly evolved in time from the K_{590} intermediates and may be used to explore further the possible structural changes in the two photocycle models considered here.

In L_1, the orientation of the SBP perpendicular to the membrane normal and the hydrogen-bond with water W_C is maintained during the annealing. Most importantly, L_1 allows for proton transfer from the Schiff base to Asp-85: the network of hydrogen-bonds formed by water molecules in the binding site, to which both the SBP and Asp-85 are connected, provides a clear path to transfer the proton. The orientation of the Schiff base with its proton perpendicular to the membrane normal allows for it to connect to the hydrogen-bond chain, which would not be possible with the SBP pointing toward Asp-96. The decrease in the distance between the Asp-85 carboxyl and the SBP from bR_{568} to L_1 fits well with proton transfer to Asp-85, as opposed to Asp-212; the SBP−Asp-212 carboxyl distance does not change much from bR_{568} to L_1.

In L_2, both carboxyl groups from Asp-85 and Asp-212 move closer to the SBP by 0.5 and 2.1 Å, respectively (relative to K_{590}). For this 13,14-*dicis* L_{550} state, the SBP is still oriented toward the extracellular side of the membrane and maintains a connection to the water molecule hydrogen-bond complex in the vicinity of the counterion. This allows the L_2 structure to contain a direct pathway for proton transfer from the Schiff base to Asp-85, as is also available in the L_1 structure. A large difference between L_1 and L_2, besides the isomerization state of retinal, is the distance of the SBP to the counterion residues. In L_1, Asp-85 is the closest group to the SBP, while, in L_2, Asp-212 is much closer (by 2 Å).

Recent FTIR data suggest that structural changes occur in the vicinity of Asp-96 during the bR → L_{550} transition.[57,69,70] Our simulations reveal a weakening of a hydrogen-bond which exists between the Asp-96 carboxyl and Lys-41 both for L_1 and L_2. L_1 shows agreement with FTIR data on changes to the retinal binding site, which suggest stronger hydrogen-bonding to the Schiff base $N-H^+$ in L_{550} as compared to bR_{568}[71] and indicate that by the formation of L_{550} a water molecule is hydrogen-bonded with both the Schiff base and Asp-85,[20,22] resulting in a distorted 13-*cis* chromophore. We found that in L_1, the hydrogen-bond interaction between the Schiff base and its proximal water molecule is considerably stronger than the Schiff base−water hydrogen-bond in bR_{568}, while the opposite is true for L_2. As stated above, this strong hydrogen-bond maintains in L_1 the orientation of the Schiff base. In L_2, a strong hydrogen-bond is not necessary to keep the SBP near the counterion region, since the *all-trans* → 13,14-*dicis* isomerization provides this orientation naturally.

Retinal Motion during $bR_{568} \rightarrow J_{625} \rightarrow K_{590} \rightarrow L_{550}$: Which Model Correlates Better with Experiment? The key question arises, which photoproduct, case 1, case 2, or case 3, represents most closely the actual structure of bR during the early steps of the photocycle? For the two isomerization models, case 1 or 2 structures primarily result from 13-*cis* simulations, and case 3 or 4 structures primarily result from 13,14-*dicis* simulations. It is useful to consider the question posed for each model separately.

Case 1 photoproducts occur most frequently for the 13-*cis* model, both at 300 K and at 77 K. If one identifies the average structure at 500 fs with the J_{625} intermediate and that at 5 ps with the K_{590} intermediate, little change can be noted between J_{625} and K_{590}. The K_{590} structure also does not explain how the Schiff base can transfer a proton to Asp-85 at a later stage. Case 2 photoproducts, on the other hand, provide a pathway for this proton transfer, via water molecule W_C. The function of water W_C is crucial; our simulations demonstrate that W_C has a profound effect on the photoreaction of retinal, stabilizing the $N-H^+$ bond in a particular orientation and opening a pathway for proton transfer. The resulting L_{550} structure, i.e., L_1, also favors proton transfer to Asp-85, since Asp-85 draws closer to the SBP in going from K_1 to L_1.

The motion of retinal during the photoisomerization is shown in Figure 14 at 500 fs intervals for the first 1.5 ps of a simulation which resulted in case 2 photoproducts. The figure demonstrates that single-bond torsions participate in the isomerization, such that retinal assumes eventually a strained configuration with the $N-H^+$ bond pointing sideways, i.e., neither to the cytoplasmic nor to the extracellular side. The final retinal geometry is stabilized through the interaction of the SBP with water W_C. This strain may be of functional importance; it might be released only after proton transfer from the Schiff base to Asp-85 (and concomitant weakening of the interaction with W_C), such that in the M_{412} intermediate the $N-H^+$ bond points toward Asp-96 from where it receives a proton. Figure 15 summarizes the suggested binding site motion for the early intermediates $bR_{568} \rightarrow J_{625} \rightarrow K_{590} \rightarrow L_{550}$. The figure points to an important role played by water in our simulations: it stabilizes the strained retinal geometry of the early intermediates, it provides the proton transfer path from retinal to Asp-85, and it is suitably placed in the retinal−Asp-96 interstitial space to provide a transfer route for water in the later part of bR's proton pump cycle. It should be emphasized that waters were not placed in the refinement reported in ref 23 to accommodate the mechanism described; rather this mechanism emerged after the refinement had been completed.

It is of interest to contrast the early intermediates simulated at room temperature with those simulated at 77 K. While case 1 occurs with higher frequency than case 2 at 300 K, the absolute ratios might not be as significant as the fact that case 2 does not occur at all at 77 K, while case 1 occurs very often. This behavior might provide a clue as to why at low temperatures (180 K) bR irradiation does not produce a high yield of M_{412} following temperature elevation: the path to case 2 photoproducts might be blocked at low temperature, such that only case 1 photoproducts develop. However, the case 1 photoproducts cannot form the M_{412} intermediate, since they do not exhibit a proton pathway to Asp-85. In this respect, it is interesting to note that irradiation of bR at 180 K detected a significantly lower yield of M_{412} upon warming.[72,73] It was suggested that at low temperatures there is a branching reaction at the L_{550} stage, such that the formation of M_{412} is inhibited and L_{550} reverts thermally to the parent pigment. This might be due to pure temperature effects on the two alternative pathways or to different K_{590} structures, as suggested by our simulations. Alternatively, it is possible that M_{412} is not accumulated, since the rates of its formation and decay are similar. The blockage of case 2 photoproducts might be due to a reduced mobility of the water molecules or of the surrounding residues. This suggestion is corroborated by the difference in the absorption maxima of the K_{590} intermediate at 300 and 77 K, as well as

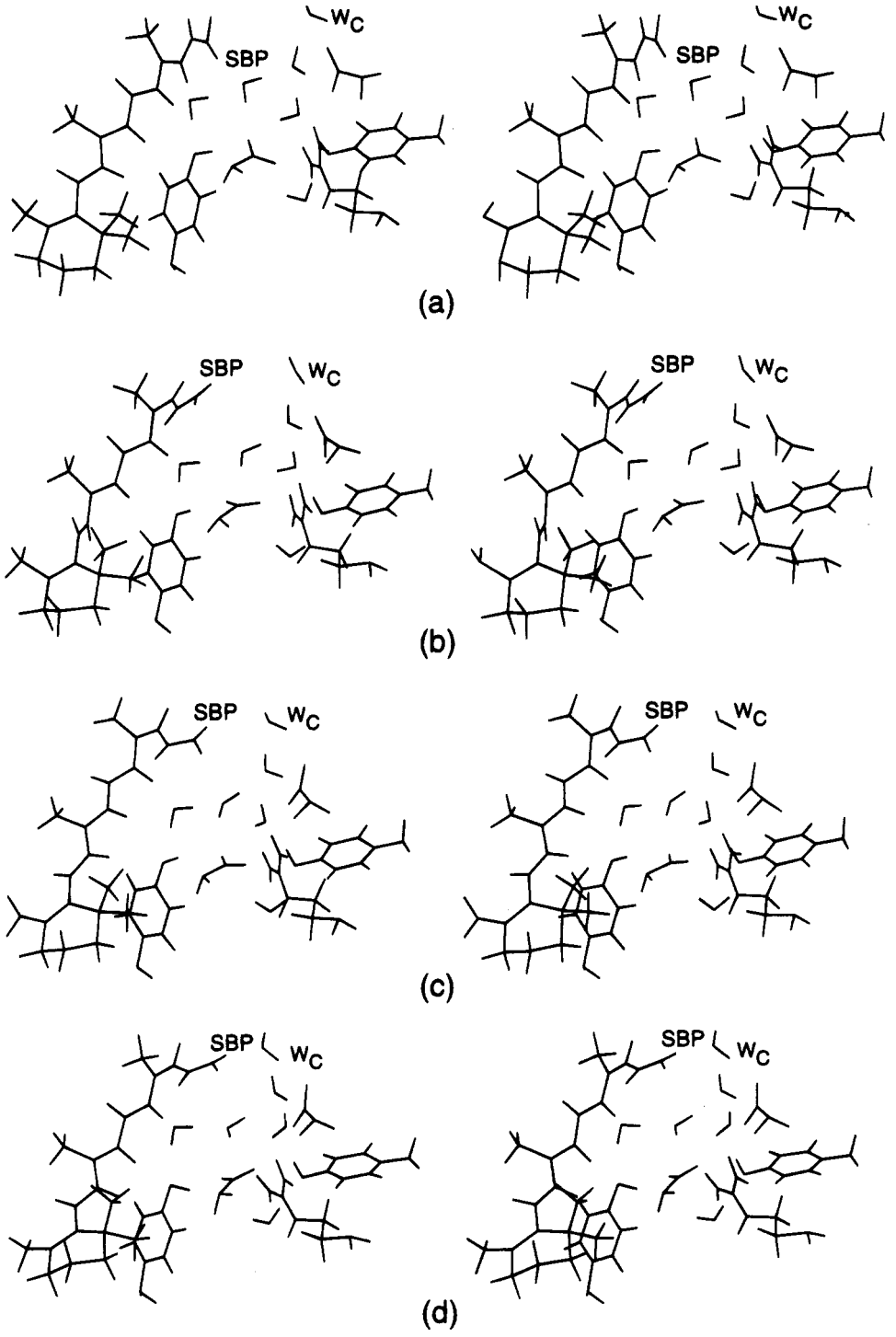

Figure 14. Stereo images of the retinal binding site during a case 2 photoisomerization simulation: (a) $t = 0$ ps; (b) $t = 0.5$ ps; (c) $t = 1.0$ ps; (d) $t = 1.5$ ps. During this interval, retinal converts from *all-trans* (a) to 13-*cis*, with a hydrogen-bond between the SBP and water W_C (d).

by the difference in the resonance Raman spectra of these two K_{590} intermediates. This suggestion is in conflict, however, with the observed quantum yield, which is temperature-independent to as low as 108 K;[61] again, the quantum yields for the reactions to case 1 and case 2 structures could be similar, with the same fraction of bR returning to *all-trans* from the S_1 excited state.

Several mutants of bR have been studied in recent years, many of which contain reduced proton-pumping activity and some of which can be induced to pump protons in the opposite direction, for example, D85T.[74] It would be of interest to apply the simulations reported here to such mutants and investigate if the occurrence of case 2 structures correlates with the mutants' proton-pumping activity. In particular, one would expect that the occurrence of case 1 structures, with $N-H^+$ pointing toward Asp-96, correlates with proton pumping in the cytoplasmic direction. Respective simulations are currently in progress.

We finally compare the behavior of retinal governed by an excited state potential favoring 13,14-*dicis* photoproducts. For this potential, a large percentage of simulations failed to isomerize at all; of the remaining cases, only half the photoproducts assumed a 13,14-*dicis* geometry. The 13,14-*dicis* structure itself (case 3) certainly contains attributes which fit well with proton transfer to Asp-85, since the SBP remains connected to the counterion region hydrogen-bond network. The simulated low-temperature behavior suggests a strong increase of case 3 products, which cannot be reconciled with observations. However, this alone would not argue strongly against the 13,14-*dicis* model. Our strongest argument against this

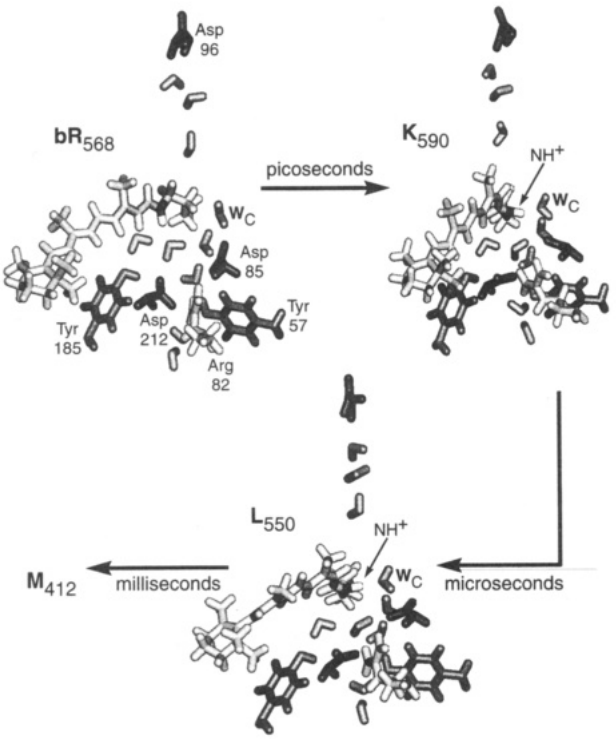

Figure 15. Suggested structures of early intermediates in the bacteriorhodopsin photocycle, $bR_{568} \rightarrow J_{625} \rightarrow K_{590} \rightarrow L_{550}$.

model actually stems from a separate study,[75] which showed that only an M_{412} intermediate formed from the L_1 intermediate induced the observed tilt of the F helix[76] and the observed shift of C_{20} of retinal.[77]

Conclusions

The present study is an attempt to delineate from the model of bacteriorhodopsin, which resulted from electron microscopy data,[11] the mechanism of this protein. In earlier studies we had complemented the model through refinement efforts, adding loop regions of bR, optimizing side group and helix placements, and, in particular, adding internal water molecules. Molecular dynamics simulations reported here built on the refined model and showed how various properties of retinal and of its immediate protein environment can control the initial photoisomerization process. The simulations revealed that details of the excited state potential surface involving carbons C_{13}, C_{14}, and C_{15} are crucial determinants of bR's photoisomerization products, the nature of which determines the mechanism of bR's proton pump cycle. Careful quantum chemical calculations of the potential surface, possibly of several closely lying surfaces, are critical for further progress in our understanding of the mechanism of bacteriorhodopsin.

The simulations presented here indicate also that the crossing from retinal's excited state to its ground state potential surface controls the quantum yield of bR's phototransformation. An excited state surface which is symmetric between the *all-trans* and 13-*cis* retinal isomers together with an instantaneous transfer to the ground state after 250 fs of excited state dynamics underestimates grossly the quantum yield of the *all-trans* $\rightarrow$ 13-*cis* photoisomerization. The observation of a very high quantum yield for the photoinduced back-reaction $K_{590} \rightarrow bR_{568}$ is also indicative of an asymmetry in the potential function and, hence, in the crossing from the excited state to the ground state surface. In the present study it was necessary to enforce an asymmetric crossing through a phase II potential surface, as depicted in Figures 4 and 5. It is possible that the phase II potential needed to bring about sufficiently large quantum yields reflects the complex nature of the potential surface crossing in retinal, which involves a variety of non-Born−Oppenheimer terms and might require a detailed quantum mechanical description. Such a description has been provided, e.g., for the isomerization of *cis*-hexatriene.[78]

An important outcome of our simulations has been the stochastic character of bR's photoreaction. Earlier descriptions[22,53] had enforced a complete photoisomerization through a respective force field such that all simulations lead to a unique K_{590}-like intermediate. The use of a more genuine excited state potential surface in the present simulations allowed us to study systematically the effect of different initial conditions on the photoreaction. Of course, the well-known quantum yield of bR of 0.64 ± 0.04,[45−47] i.e., a value significantly less than unity, also indicates that bR's photoisomerization has strong probabilistic attributes. Our simulations indicate, actually, that there do not only exist two outcomes of bR's photoreaction, i.e., *all-trans*-retinal corresponding to bR and 13-*cis*-retinal corresponding to K_{590}, but rather four outcomes (see Table 4 and Figure 8). Reports in the literature of inactive photocycles of bR[64] and the observation that bR mutants can produce proton currents directed toward the cytoplasmic side[74] appear to point also to a possible side reaction after the photoisomerization. Nevertheless, the different outcomes of the simulated photoreaction in our study have been a surprise which deserves further experimental and theoretical investigations. Such investigations will also require a better, i.e., accurate quantum chemical, description of the excited state potential surfaces of retinal.

Despite the uncertainties of the excited state potential employed here, a definite candidate for the K_{590} intermediate emerged from our simulations. This candidate, shown in Figure 15, involves an $N-H^+$ bond pointing in a direction orthogonal to bR's long axis, stabilized by a water molecule which connects the SBP to Asp-85. This intermediate is ideally suited to realize the switch needed to explain the proton pump mechanism of bR: transfer of the SBP to Asp-85 weakens the interaction of the Schiff base nitrogen with the mentioned water such that torsional strains in retinal lead to a reorientation of the Schiff base, leaving the nitrogen pointing toward Asp-96.

If one accepts our suggestion for the identity of the K_{590} intermediate, the conclusion can be drawn from our study that neither the J_{625} intermediate nor the L_{550} intermediate is structurally very distinct from the K_{590} state; during the time course of the $J_{625} \rightarrow K_{590} \rightarrow L_{550}$ transitions, as described in simulations $A1_{300}...A50_{300}$ and simulation C, retinal and the protein experience a structural relaxation but no distinct and functionally significant transformation.

The most compelling result is the participation of water in the early stages of bR's pump cycle. A water molecule plays the pivotal role of stabilizing the early retinal intermediate in a strained geometry and furnishes a proton transfer pathway. Our investigation emphasizes the need to identify the location of water molecules in bR either through observation, e.g., through two-dimensional NMR spectra with water−amino acid cross peaks, or through improved modeling, e.g., through free energy perturbation calculations determining optimal water location in bR. Even though considerable progress has been achieved in sharpening the focus of investigations on the proton pump mechanism of bR, the present investigation has raised more questions than it has provided answers.

Acknowledgment. The authors wish to thank Ilya Logunov for calculation of retinal partial charges and dihedral angle parameters. All simulations were carried out using Hewlett-Packard 735 workstations operated by the Resource for Concurrent Biological Computing at the University of Illinois and Beckman Institute. This work was supported by grants from

the National Institutes of Health (PHS 5 P41 RR05969-04), the National Science Foundation (BIR-9318159), and the Roy J. Carver Charitable Trust.

References and Notes

(1) Permanent address: Department of organic chemistry, the Weizmann Institute of Science, Rehovot 76100, Israel.

(2) To whom correspondence should be addressed. Email: kschulte@ks.uiuc.edu.

(3) Abbreviations used: bR, bacteriorhodopsin; EM, electron microscopy; FTIR, Fourier transform infrared; HOOP, hydrogen-out-of-plane; SBP, Schiff base proton.

(4) Khorana, H. G. *J. Biol. Chem.* **1988**, *263*, 7439.

(5) Birge, R. R. *Annu. Rev. Phys. Chem.* **1990**, *41*, 683.

(6) Mathies, R. A.; Lin, S. W.; Ames, J. B.; Pollard, W. T. *Annu. Rev. Biochem. Bioeng.* **1991**, *20*, 491.

(7) Lanyi, J. K. *J. Bioenerg. Biomembr.* **1992**, *24*, 169.

(8) Oesterhelt, D.; Tittor, J.; Bamberg, E. *J. Bioenerg. Biomembr.* **1992**, *24*, 181.

(9) Ebrey, T. Light energy transduction in bacteriorhodopsin. In *Thermodynamics of Membranes, Receptors and Channels;* Jacobson, M., Ed.; CRC Press: New York, 1993; p 353.

(10) Lozier, R. H.; Bogomolni, R. A.; Stoeckenius, W. *Biophys. J.* **1975**, *15*, 955.

(11) Henderson, R.; Baldwin, J. M.; Ceska, T. A.; Zemlin, F.; Beckmann, E.; Downing, K. H. *J. Mol. Biol.* **1990**, *213*, 899.

(12) Papadopoulos, G.; Dencher, N.; Zaccai, G.; Büldt, G. *J. Mol. Biol.* **1990**, *214*, 15.

(13) de Groot, H. J. M.; Harbison, G. S.; Herzfeld, J.; Griffin, R. G. *Biochemistry* **1989**, *28*, 3346.

(14) de Groot, H. J. M.; Smith, S. O.; Courtin, J.; van den Berg, E.; Winkel, C.; Lugtenburg, J.; Griffin, R. G.; Herzfeld, J. *Biochemistry* **1990**, *29*, 6873.

(15) Rothschild, K. J.; Braiman, M. S.; He, Y. W. *J. Biol. Chem.* **1990**, *265*, 16985.

(16) Needleman, R.; Chang, M.; Ni, B.; Varo, G.; Fornes, J.; White, S. H.; Lanyi, J. K. *J. Biol. Chem.* **1991**, *266*, 11478.

(17) Dupuis, P.; Harosi, F.; Sandorfy, C.; Leclercq, J. M.; Vocelle, D. *Rev. Can. Biol.* **1980**, *39*, 247.

(18) Hildebrandt, P.; Stockburger, M. *Biochemistry* **1984**, *23*, 5539.

(19) Gat, Y.; Sheves, M. *J. Am. Chem. Soc.* **1993**, *115*, 3772.

(20) Maeda, A.; Sasaki, J.; Yamazaki, Y.; Needleman, R.; Lanyi, J. K. *Biochemistry* **1994**, *33*, 1713.

(21) Kandori, H.; Yamazaki, Y.; Sasaki, J.; Needleman, R.; Lanyi, J. K.; Maeda, A. *J. Am. Chem. Soc.* **1995**, *117*, 2118.

(22) Zhou, F.; Windemuth, A.; Schulten, K. *Biochemistry* **1993**, *32*, 2291.

(23) Humphrey, W.; Logunov, I.; Schulten, K.; Sheves, M. *Biochemistry* **1994**, *33*, 3668.

(24) Parodi, L. A.; Lozier, R. H.; Bhattacharjee, S. M.; Nagle, J. F. *Photochem. Photobiol.* **1984**, *40*, 501.

(25) Schulten, K.; Schulten, Z.; Tavan, P. An isomerization model for the pump cycle of bacteriorhodopsin. In *Information and Energy Transduction in Biological Membranes*; Bolis, L., Helmreich, E. J. M., Passow, H., Eds.; Allan, R. Liss, Inc.: New York, 1984; p 113.

(26) Váró, G.; Lanyi, J. K. *Biochemistry* **1990**, *29*, 2241.

(27) Gerwert, K.; Souvignier, G.; Hess, B. *Proc. Natl. Acad. Sci. U.S.A.* **1990**, *87*, 9774.

(28) Sharkov, A. V.; Pakulev, A. V.; Chekalin, S. V.; Matveetz, Y. A. *Biochim. Biophys. Acta* **1985**, *808*, 94.

(29) Polland, H.; Franz, M. A.; Zinth, W.; Kaiser, W.; Kölling, E.; Oesterhelt, D. *Biophys. J.* **1986**, *49*, 651.

(30) Petrich, J. W.; Breton, J.; Martin, J. L.; Antonetti, A. *Chem. Phys. Lett.* **1987**, *137*, 369.

(31) Milder, S. J.; Kliger, D. S. *Biophys. J.* **1988**, *53*, 465.

(32) Tsuda, M.; Galccum, M.; Nelson, B.; Ebrey, T. G. *Nature* **1980**, *287*, 351.

(33) Braiman, M.; Mathies, R. *Proc. Natl. Acad. Sci. U.S.A.* **1982**, *79*, 403.

(34) Atkinson, G. H.; Brack, T. L.; Blanchard, D.; Rumbles, G. *Chem. Phys.* **1989**, *131*, 1.

(35) Doig, S. J.; Reid, P. J.; Mathies, R. A. *J. Phys. Chem.* **1991**, *95*, 6372.

(36) Hudson, B. S.; Kohler, B. E.; Schulten, K. Linear polyene electronic structure and potential surfaces. In *Excited States*; Lim, E. C., Ed.; Academic Press: New York, 1982; Vol. 6, p 1.

(37) Warshel, A.; Barboy, N. *J. Am. Chem. Soc.* **1982**, *104*, 1469.

(38) Warshel, A.; Chu, Z. T.; Hwang, J.-K. *Chem. Phys.* **1991**, *158*, 303.

(39) Smith, S. O.; Hornung, I.; van der Steen, R.; Pardoen, J. A.; Braiman, M. S.; Lugtenburg, J.; Mathies, R. A. *Proc. Natl. Acad. Sci. U.S.A.* **1986**, *83*, 967.

(40) Fodor, S. P. A.; Ames, J. B.; Gebhard, R.; Berg, E. M. M. v. d.; Stoeckenius, W.; Lugtenburg, J.; Mathies, R. A. *Biochemsitry* **1988**, *27*, 7097.

(41) Schulten, K.; Tavan, P. *Nature* **1978**, *272*, 85.

(42) Schulten, K. An isomerization model for the photocycle of bacteriorhodopsin. In *Energetics and Structure of Halophilic Organisms*; Caplan, S. R., Ginzburg, M., Eds.; Elsevier: Amsterdam, 1978; p 331.

(43) Orlandi, G.; Schulten, K. *Chem. Phys. Lett.* **1979**, *64*, 370.

(44) Gerwert, K.; Siebert, F. *EMBO J.* **1986**, *4*, 805.

(45) Schneider, G.; Diller, R.; Stockburger, M. *Chem. Phys.* **1989**, *131*, 17.

(46) Govindjee, R.; Balashov, S. P.; Ebrey, T. G. *Biophys. J.* **1990**, *58*, 597.

(47) Tittor, J.; Oesterhelt, D. *FEBS Lett.* **1990**, *263*, 269.

(48) Bashford, D.; Gerwert, K. *J. Mol. Biol.* **1992**, *224*, 473.

(49) Jorgensen, W. L.; Chandrasekhar, J.; Madura, J. D.; Impey, R. W.; Klein, M. L. *J. Chem. Phys.* **1983**, *79*, 926.

(50) Brünger, A. T. *X-PLOR.* The Howard Hughes Medical Institute and Department of Molecular Biophysics and Biochemistry, Yale University, New Haven, CT, May 1988.

(51) Brooks, B. R.; Bruccoleri, R. E.; Olafson, B. D.; States, D. J.; Swaminathan, S.; Karplus, M. *J. Comput. Chem.* **1983**, *4*, 187.

(52) Frisch, M. J.; Trucks, G. W.; Head-Gordon, M.; Gill, P. M. W.; Wong, M. W.; Foresman, J. B.; Johnson, B. G.; Schlegel, H. B.; Robb, M. A.; Replogle, E. S.; Gomperts, R.; Andres, J. L.; Raghavachari, K.; Binkley, J. S.; Gonzalez, C.; Martin, R. L.; Fox, D. J.; Defrees, D. J.; Baker, J.; Stewart, J. J. P.; Pople, J. A. *Gaussian 92,* Revision A; Gaussian Inc.: Pittsburgh, PA, 1992.

(53) Nonella, M.; Windemuth, A.; Schulten, K. *J. Photochem. Photobiol.* **1991**, *54*, 937.

(54) Laarhoven, P. J. M. v.; Aarts, E. H. L. *Simulated Annealing: Theory and Application;* D. Reidel: Dordrecht, 1987.

(55) Brünger, A. *Annu. Rev. Phys. Chem.* **1991**, *42*, 197.

(56) Ryckaert, J.-P.; Ciccotti, G.; Berendsen, H. J. C. *J. Comput. Phys.* **1977**, *23*, 327.

(57) Braiman, M. S.; Mogi, T.; Marti, T.; Stern, L. J.; Khorana, H. G.; Rothschild, K. J. *Biochemsitry* **1988**, *27*, 8516.

(58) Becher, B.; Tokunaga, F.; Ebrey, T. G. *Biochemistry* **1978**, *17*, 2293.

(59) Scharnagl, C.; Hettenkofer, J.; Fisher, S. *J. Phys. Chem.* **1995**, *99*, 7787.

(60) Engels, M.; Gerwert, K.; Bashford, D. *Biophys. Chem.*, in press.

(61) Balashov, S. P.; Imasheva, E. S.; Govindjee, R.; Ebrey, T. G. *Photochem. Photobiol.* **1991**, *54*, 955.

(62) Diller, R.; Stockburger, M. *Biochemistry* **1988**, *27*, 7641.

(63) Wu, S.; El-Sayed, M. A. *Biophys. J.* **1991**, *60*, 190.

(64) Eisfeld, W.; Pusch, C.; Diller, R.; Lohrmann, R.; Stockburger, M. *Biochemistry* **1993**, *32*, 7196.

(65) Xu, D.; Martin, C.; Schulten, K. Molecular dynamics study of the early picosecond events in the bacteriorhodopsin photocycle: Dielectric response, vibrational cooling and the J, K intermediates. Submitted to *Biophys. J.*

(66) Balashov, S. P.; Karneyeva, N. V.; Litvin, F. F.; Ebrey, T. G. *Photochem. Photobiol.* **1991**, *54*, 949.

(67) Cury, B.; Pallings, I.; Brock, A.; Pardoen, J.; Lugtenburg, J.; Mathies, R. *Adv. Infrared Raman Spectrosc.* **1985**, *12*, 115.

(68) Gat, Y.; Grossjean, M.; Pinevsky, I.; Takei, H.; Rothman, Z.; Sigrist, H.; Lewis, A.; Sheves, M. *Proc. Natl. Acad. Sci. U.S.A.* **1992**, *89*, 2434.

(69) Gerwert, K.; Hess, B.; Soppa, J.; Oesterhelt, D. *Proc. Natl. Acad. Sci. U.S.A.* **1989**, *86*, 4943.

(70) Maeda, A.; Sasaki, J.; Shishida, Y.; Yoshizawa, T.; Chang, M.; Ni, B.; Needleman, R.; Lanyi, J. K. *Biochemistry* **1992**, *31*, 4684.

(71) Maeda, A.; Sasaki, J.; Pfefferlé, J.; Shichida, Y.; Yoshizawa, T. *Photochem. Photobiol.* **1991**, *54*, 911.

(72) Kalisky, O.; Ottolenghi, M.; Honig, B.; Korenstein, R. *Biochemistry* **1981**, *20*, 649.

(73) Kalisky, O.; Ottolenghi, M. *Photochem. Photobiol.* **1982**, *35*, 109.

(74) Tittor, J.; Schweiger, U.; Oesterhelt, D.; Bamberg, E. *Biophys. J.* **1994**, *67*, 1682.

(75) Xu, D.; Sheves, M.; Schulten, K. Molecular dynamics study of the M intermediate of bacteriorhodopsin. Submitted to *Biophys. J.*

(76) Subramanian, S.; Gerstein, M.; Oesterhelt, D.; Henderson, R. *EMBO J.* **1993**, *12*, 1.

(77) Heyn, M. P.; Otto, H. *Photochem. Photobiol.* **1992**, *56*, 1105.

(78) Olivucci, M.; Bernardi, F.; Celani, P.; Ragazos, I.; Robb, M. A. *J. Am. Chem. Soc.* **1994**, *116*, 1077.

JP951470W